IOP Conference Series: Materials Science and Engineering

PAPER • **OPEN ACCESS**

CAE applications in a thermoforming mould design

To cite this article: AR Marjuki *et al* 2016 *IOP Conf. Ser.: Mater. Sci. Eng.* **114** 012012

View the article online for updates and enhancements.

Related content

- Numerical investigation of wrinkle for multi-point thermoforming of Polymethylmethacrylate sheet
Heli Peng, Haijian Liu and Xiaolong Zhang
- Application of alcohol based spraying coating on green sand mould for steel casting
Z L Xu, J Wang, S S Yang et al.
- Utilizing of inner porous structure in injection moulds for application of special cooling method
M Seidl, J Bobek, J Šafka et al.

This content was downloaded from IP address 103.53.34.15 on 28/05/2018 at 08:40

IOP Conf. Series: Materials Science and Engineering **114** (2016) 012012 doi:10.1088/1757-899X/114/1/012012

CAE applications in a thermoforming mould design

AR Marjuki[1], FA Mohd Ghazali[1], N M Ismail[1], S Sulaiman[1], I Mohd Khairuddin[1], Anwar P P A[1] Majeed, AA Jaafar[1], F Mustapha[2] and S Basri[1]

[1] Fac of Manufacturing Eng, Universiti Malaysia Pahang, 26600, Pekan Pahang, Malaysia
[2] Dept of Aerospace Eng, Fac of Eng, Universiti Putra Malaysia, Serdang 43400, Selangor, Malaysia

E-mail: ensaaj@ump.edu.my

Abstract. Preparation of honeycomb layer is a critical step for successful fabrications of thermoformed based sandwiched structures. This paper deals with an initial investigation on the rapid manufacturing process of corrugated sheet with 120° dihedral angles. Time history of local displacements and thickness, assuming viscous dominated material model for a 1mm thick thermoformable material, was computed by using ANSYS® Polyflow solver. The quality of formed surfaces was evaluated for selection of mould geometry and assessment of two common variants of thermoforming process. Inadequate mesh refinement of a membrane elements produces satisfactorily detailing and incomplete forming. A perfectly uniform material distribution was predicted using drape forming process. However, the geometrical properties of vacuum formed part are poorly distributed and difficult to control with increasing inflation volumes. Details of the discrepancies and the contributions of the CAE tool to complement traditional trial and error methodology in the process and design development are discussed.

1. Introduction

In modern thermoforming manufacturing practices, prototype evaluation activity is an important step in the design process. Effective assessment may require complete understanding on the details of the manufacturing process. Following Throne (2008), the drape and vacuum forming processes begin by positioning a mould over a platen. A thermoformable blank material is clamped to a holding frame and heated up to a forming temperature. The transfer stage is where the heated blank material is brought into contact with the platen at a designated approaching speed. The forming stage is immediately initiated by evacuating the air between the mould and the blank material for forming processes. Cooling stage is where the formed part is left cooled to retain the final shape and then it is removed from mould as part of the removal stage. Computer Aided Engineering (CAE) are extensively applied to optimize these stages to fulfill many demanding objective and cost functions. Computer simulations may also be used to examine product robustness with the availability of new material and technology. During the last few decades CAE has been a valuable tool to the thermoforming industries. A variety of products have been produced to reach wider industrial needs. Integration of advanced numerical methods, traditional trial and error approaches and the downstream predictive technologies such as process optimization and machine learning method have made further improvement on the product development. To date detail implementation of finite element analysis (FEA) for thermoforming thin gauge thermoformable material is continuously reported in the open literatures. A generic


Content from this work may be used under the terms of the Creative Commons Attribution 3.0 licence. Any further distribution of this work must maintain attribution to the author(s) and the title of the work, journal citation and DOI.
Published under licence by IOP Publishing Ltd

material were also studied for various reasons. Kershner and Glacomin (2007) for example determined Lagrangian properties by solving the continuity and momentum equations that govern the constrained inflation of a Newtonian fluid over a truncated cone surfaces of a negative mould. The near melt states were assumed for the thermo-mechanical properties. Total forming, forming and contrained forming times and intervals were approximated by using a thin film approximations. It was shown that the blank material gradually evolves from flat to either lenticular or bulbous shapes according to the cone angle. The analytical solutions proved that the detailing or thermoform sharp edges and corners are practically difficult to achieved. Pepliński and Mozer (2011) modeled a 1mm thick blank material as a fluid membrane as the thickness was two order of magnitude lower than the other dimension. ANSYS® Polyflow solver was used to simulate vacuum forming process of a rotationally symmetric cup. The near melt density and dynamic viscosity of the blank material were set to 900 kg/m^3 and 8630 Pa.s respectively. The approaching speed during transfer stage was 50 mm/s and the inflation phase was maintained at 500kPa forming pressure. The blank material was meshed with 3-nodes triangular membrane element and the part quality was determined by a minimum wall thickness of 0.3mm. With the advances in constitutive modeling, various material models were proposed to improve the predictions of the nonlinear deformation behavior of thin gauge thermoplastics materials during the inflation phase. Karamanao et al(2006) approximated the behavior of a generic thin gauge thermoformable material as a finite viscoelastic material. Constitutive modeling using a finite deformation generalization of a spring and dashpot material model relates the internal stress state with the entire history of material deformation. Computer simulations were carried out using a high temperature incompressible membrane element that can sustain no bending moments. Detailing predictions were reported with a residual based error estimator for mesh refinement strategy. The algorithm was used to adaptively identify large deformable membrane element and those in the proximity of complex contact surfaces. Good surface replication when multiple plane point transition corners are refined with adequate density of computational mesh. Dong et al (2006) models the acrylic as a hyperelastic Mooney-Rivlin and Ogden material with path-independent characteristics. A dynamic explicit theory incorporated in a commercial code PAM-FORM® were selected with an automatic selective adaptive and uniform remeshing mesh refinement algorithms.The blank material was meshed with 4-node quadrilateral thin flat shell elements which capable of out of plane deformation. A prescribed angle between elements to trigger complex surface contour was used as the criteria for automatic selective adaptive grid refinement. A uniform mesh refinement algorithm was also applied in a defined adaptive region domain. Using typical industrial process conditions Ó Connor et al (2013) simulated the behavior of a 1.23mm thick polypropelene during the forming phase using a 3-node thick axisymmetric thermo-mechanically coupled shell elements that allow in-plane deformation and temperature gradient. A constitutive equation for a large deformation thermally coupled viscoelastic material model was proposed to allow heat loss during the forming processes. A multiphysics strategy in simuli ABACUS/Standard was adopted to determine the total pressurised phase by using a computational fluid dynamic approach. A plug-assisted vacuum forming was simulated for rotationally symmetric receptacle. An adaptive mesh algorithm was applied to modify the mesh density at location where considerable material straining and rapid changes of surface geometry. Realistic contact force and material distribution was achieve with adequate number of contact element to resolve the mould surface curvature. Lupea and Cormier(2007) assumed that the behavior of an energy absorbing material SafetyPlastic® can be represented by an elasto-plastic material. A drape forming process of a truncated cone was simulated using a commercial nonlinear finite element solver LS Dyna and ® with a 4-node quadrilateral MAT19, MAT24 and MAT81 shell elements. Denser mesh was located in the circumferential direction. Kittikanjanaru and Patcharaphun (2013) examined a 1mm thick HIPS and A-PET with density of 1040 and 1370 kg/m^3 respectively. Both materials were assumed to behave as a visco elastic

K-BKZ non-linear and time-independent material during a drape and vacuum forming of a truncated cone and a food tray. The computations were carried out using a nonlinear finite element solver T-SIM® with 3-node triangular shell elements. The study assessed the forming process from the predicted material distribution. Chevaugeon et al (2000) studied a fibers-reinforced thermoplastic behavior during drape forming process of circular mould. The behavior of the blank material was represented by a hyperelastic traversely isotropic material and the simulation was made by using 3-node isoparametrical triangular flat membrane elements that deform in out-of plane direction. An automatic remeshing algorithm of the nonlinear finite element solver T-SIM® allocated denser mesh in high curvature region at the adiabatic and rigid contact surfaces. Thicker part was predicted at the flange of the formed part and thinner at the mould edges. Erchiqui et al (2005) treated a 1.6mm thick ABS as an isotropic incompressible thermoplastic material. The viscoelastic integral of Lodge and Christensen material models, and the hyperelastic Mooney-Rivlin and Ogden material model were assessed for large deformation with finite strain and plane stresses. With 1.0s blow time, drape forming process was simulated using a specific purpose built dynamic explicit finite element solver Thermoform that capable to resolve exponentially rapid changes in the solution components. The blank material was meshed with 3-node isothermal isoparametric plate elements. Peng et al (2012) treated a 2.75mm thick wood polypropelene composites thermoviscoelastic material and modeled the elastic and viscoelastic properties of wood and polymer respectively. Drape forming of car interior part was simulated using explicit finite element solver LS Dyna with 3-node isoparametric plate elements. Thongwichean et al (2012) proposed a temperature dependence material model that was insensitive to strain rate and no strain hardening after yield. The model was configured into a finite element solver Simula Abaqus agree to simulate the behavior of a Tapioca starch biodegradable polyester blend of Enpol®TM. The blank material was meshed with 2D shell (S8) element. The approaching speed of 2.5mm/s was assumed during the transfer stages to a rigid and adiabatic mould surfaces. These studies among others not considered here implemented virtually the same numerical setup and engineering assumptions. This article is intended to complement these efforts by addressing aspects of mould design for thermoformed honeycomb core parts as shown in Figure 1. In industrial applications, the plastic products have been used for a variety of purposes such as sound and vibration damping and filtering medias. It is small in size and is characterized by simple geometrical features. Vacuum and drape thermoforming processes were simulated and it is hypothesized that the quality of the formed part will be varied with the changes in the mould design and selection of manufacturing process. The objective of the study is to conduct parametric assessment on material distribution during the forming stage of both manufacturing processes. Details engineering approach for mould design evaluation is described in the following sections. Relationship between the computed results and the formulated hypothesis is the summarized and concluded.

Table 1. Physical parameter specifications for corrugated honeycomb layer.

Geometrical property	specification
Dihedral angle $\times 10^{-3}(^o)$	120
Pitch $\times 10^{-3}$(mm)	9
Node bonds $\times 10^{-3}$(mm)	4.5
Ribbon, $l \times 10^{-3}$(mm)	120
Cell size $\times 10^{-3}$(mm)	7
thickness, $w \times 10^{-3}$(mm)	100

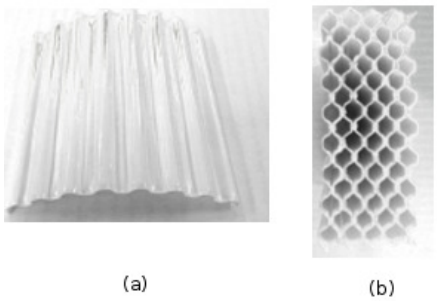

Figure 1. Pictorial images of thermoformed (a) corrugated honeycomb layer and (b) honeycomb core .

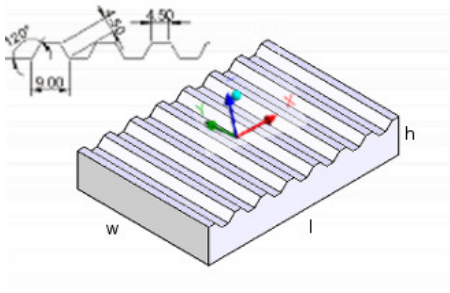

Figure 2. Schematics of corrugated pattern and perspective view of positive mould.

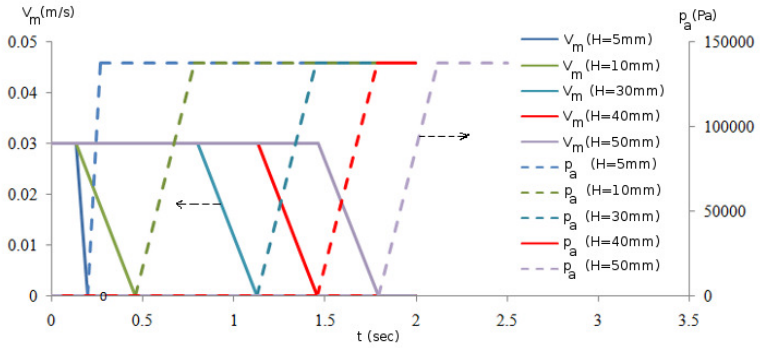

Figure 3. Design of vacuum forming process

2. Computational Model and Numerical Methods

A honeycomb layer is designed to construct a hexagonal honeycomb core as shown in Figure 1. For convenience in describing the physical model, the layer is viewed as corrugated plate with regular and periodic pattern of flat planes. These planes intersect at 2-plane point transition corners and form 120° dihedral angle . The perspective view of a positive mould and the schematics of corrugated pattern are shown in Figure 2 and its specifications are summarized in Table 1. As a basis for part quality evaluation, the engineering assumptions for the blank material and mould are briefly given as follows:

- The thermo-mechanical properties of a generic thermoformable material are evaluated at near-melt states and are assumed constant and isotropic.
- Rigid, adiabatic and smooth contact surfaces
- isothermal and rapid forming process
- aspect of mould design such as draft, vent hole, surface textures are not implemented.

The mould will be positioned at the centroid of a platen and such arrangement introduced 2- and 3-plane point transition corners and forming surfaces. The area of both platen and the pre-cut blank material are (A_i=)140x160mm^2 and the flat free surface(A_o) of 100x120mm^2. Due to symmetrical properties, the computational model is $\frac{A_i}{4}$ (=70 x80mm^2). The initial thickness of the blank material (h_i=) is 1mm. The origin of the solution domain (x=0, y=0, z=0) is located at a point where symmetry planes in x and y-directions intersect with z=0 plane.

Figure 3 shows the two consecutive stages of the forming processes. In the transfer phase, the blank material maintain an approaching speed of 30mm/s and is brought into contact with the platen at constant deceleration when the separation distance between the surfaces is 5mm. The edges of the blank material and platen remain attached and the inflation phase begin immediately by raising the air pressure. The total pressurised interval (θ_p) to bring the pressure up to a forming pressure(p_a) takes 0.5s. It is kept constant at 138kPa throughout the inflation phase(θ_i). Ideally the total manufacturing time ($\theta_T \leq \theta_i$) should be determined by the period required by the blank material to capture the entire working surface of the mould. However this is not possible in the presence of multiple -plane transitions point transition corners. In this article, all computer simulations were terminated when a prescribed number of time step is reached. The equations that governed the forming process of the blank material during these stages are derived from the Lagrangian motion of an infinitesimally small control mass in the material are given below:

$$\nabla \cdot \mathbf{v} = 0 \tag{1}$$

$$-\nabla p + \nabla \cdot \mathbf{T} + \mathbf{f} = \rho \mathbf{a} \tag{2}$$

where p, $\mathbf{T}$, $\mathbf{f}$, ρ, $\mathbf{a}$ and $\mathbf{v}$ are the Lagrangian forms of pressure, extra-stress tensor ,body force, density of 1000 kg/m^3, acceleration and velocity respectively. The continuity equation simply provide an insight that any local thinning is accompanied by a plane deformation. This is consistent by assuming that the second viscosity does not responsible to the volumetric deformation. In this article, the behavior of the blank material is represented by the Generalized Newtonian fluid material model such that $\mathbf{T}$ is defined as

$$\mathbf{T} = 2\eta \mathbf{D} \tag{3}$$

where η is the zero shear rate viscosity and take the value of 10^5 Pa.s. In the absence of contact, the kinematic conditions is given by

$$v_i = \frac{\partial x_i}{\partial t} \tag{4}$$

when the contact is established between two different surfaces, deformable-to-rigid contact is assumed whereby the local reaction force is modeled by a penalty method algorithm. The parallel and normal components of the local surface force are respectively given by

$$f_s = C_s[v(s,t) - V_m(s,t)] \tag{5}$$

$$f_n = C_n[v(n,t) - V_m(n,t)] \tag{6}$$

where C_t and C_n are known as slipping and penalty coefficients respectively and took the value of 10^{10} Ns/m. Details of the numerical implementation for solving the algebraic governing equations is given in the ANSYS® Polyflow online documentation[12]. In summary, the blank material is divided into finite membrane elements, and the governing equations are discretised using a finite element method. The surface contact force is derived by meshing the mould surfaces with finite contact elements . At the beginning of computations, 5600 membrane and 11455 contact elements took a structured distribution of 4-node quadrilateral structural elements. The ANSYS® Polyflow solver was configured to adopt an implicit Euler differencing scheme with typical minimum and maximum time steps of $1\times\ 10^{-5}$s and 0.1s respectively. In order to satisfy the rigid surface assumption, the solver was fed with a hard constraint to automatically terminate further iterative calculations on membrane deformation if the maximum

mould normal deformation of 0.05mm is reached. The transient computations were carried out on a personal computer with Intel® Core (TM) i5-2400 CPU @ 3.10GHz and 4.00 GB RAM. The Ansys ® Polyflow solver is executed on 32-bit Windows 7 Professional operating system to provide the time history of forming process up to 500 successful time step. Table 2 tabulates the test matrix for a range of mould height, H considered in the present study. Majority of the test case took at most 5400 sec of CPU times to complete.

Table 2. Test Matrix for numerical experiment: p_a=138kPa, V_m(z,0)=30mm/s, h_i=1mm, η=10^5Pa.s, ρ=1000kg/m^3, generic thermoformable material at near-melt states

	negative mould	positive mould
Mould Height(H) $\times$ 10^{-3}(m)	-50 -40 -30 -20 -10	0 10 20 30 40 50

3. Results and Discussion

This section addresses a part quality in the context of numerical result. Two main concerns are the detailing and material distribution. Acceptable predictions of material behavior are reflected by a realistic evaluation of forces at the contact location as well as the ability of the form part to perfectly replicate the surfaces of corrugated pattern with negligible dimensional uniformity of material thickness. Figure 4 are the overlay images of 3D-wireframe representation of undeformed mould and the membrane element distributions of the formed part. The red curves, which should be hidden from these views, are the locus of point transition corners and its appearances indicate unrealistic geometric penetrations at the contact location and incomplete forming. At these locations, the local membrane elements are relatively large and fail to capture the mould surfaces. These figures imply that an accurate predictions of formed part requires modifications to the mould geometry and adequate level of mesh density. The mesh properties should also take into account the stretching processes during inflation phase to prevent incomplete forming prediction. Insufficient mesh density resulted wrong topography information about the corrugated pattern and mould surfaces. In the following discussion, results of numerical experiment are presented using the same mesh density.

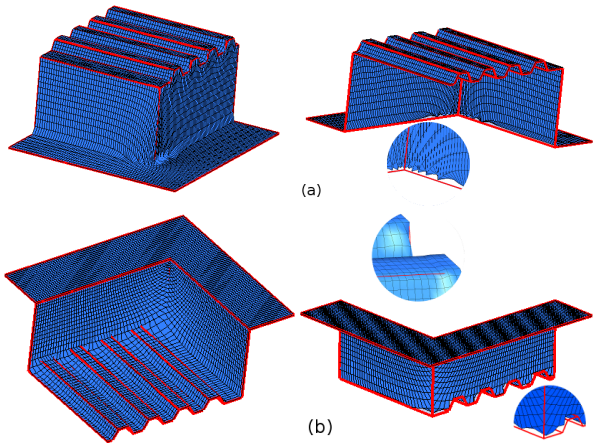

Figure 4. Front and rear views of overlaid formed part (a) on 3D wirefame 40mm positive mould (b) on 3D wirefame 40mm negative mould

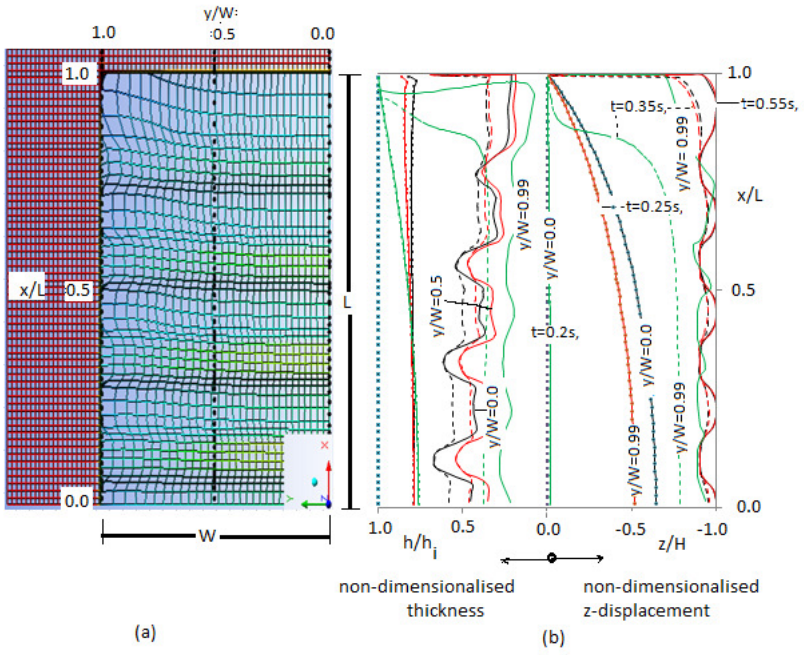

Figure 5. (a)Material deformation for H=40mm negative mould (b) time history of material distribution and z-position at plane y/W=0.0, 0.5 and 0.99 during inflation phase t $< \theta_i$=0.55s .

For convenience in the detail discussions, the time history of z-component displacement of part formed over a 40mm deep negative mould during the inflation phase of vacuum forming process is shown in Figure 5. The z-direction view shows nonuniform distribution of geometrically distorted membrane elements. The undeformed flange of the blank material indicate correct formulations of the transfer stage and an established contact between the platen and the flange. The displacement profiles suggest free inflation with lenticular shape. The nonuniformity of local displacement is more pronounce as the differential pressure raise to the p_a. The time history suggest that the internal forces has stretched the membrane elements in the direction and magnitude which depends on the h, location and the magnitude of p_a. The h of a moving membrane is progressively reduced until contact is established with the mould surfaces. Eventually the dimensional variation of h, ranging between 10 to 60 percent of h_i, can be observed in x and y direction and the patterned surface is not completely captured.

Figure 6 indicates that the vacuum formed parts have unsatisfactory spatial material distribution compared to those of drape formed parts. The nonuniformity of thickness can seen in x and y direction with variation between 10 to 70 percent of h_i. The top side of the pattern is thicker than that of the base up to 25 percent from h_i. The gradient of h is increasing at larger y/W. Figure 7 compares the material distributions of four different drape and vacuum formed parts. The arrows indicate increasing H of positive and negative moulds respectively. These results imply that the corrugated surfaces can be reproduced by both vacuum and drape thermoforming processes. For the former, good part thickness can be obtained using shallow negative mould. The material distribution varies with H and A_o and it is increasingly difficult to control the thickness uniformity as H increasing. Thinner section can be observed at the part edges and the structurally weak area is expanding with increasing H. However, The material distribution of drape formed parts does not depends on H, and h distributions are perfectly uniform. The top side has about the same thickness as h_i and h at the base side is approximately

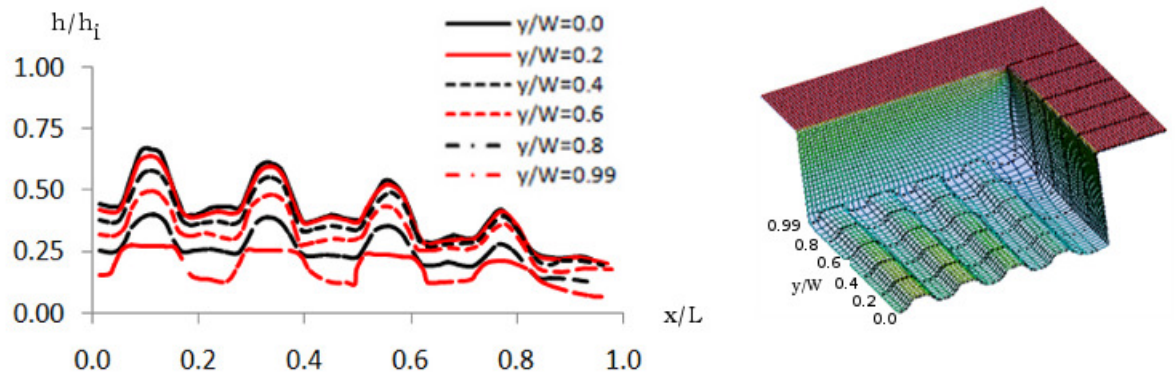

Figure 6. Spatial distributions of vacuumed form part on H=40mm negative mould at y/w = 0, 0. 2, 0.4,0.6,0.8,0.99.

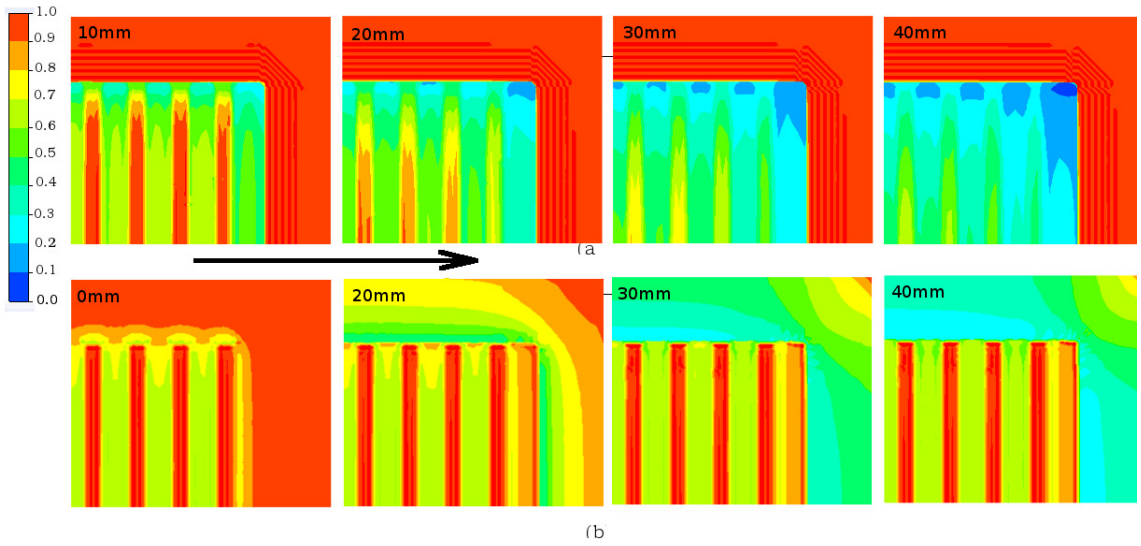

Figure 7. Material distribution of formed parts on H= 5mm, 10mm, 40mm and 50mm (a) negative mould (b) positive mould.

40 percent of h_i. As expected, thinner area is observed at the edges of positive mould and h at these location varies with H.

4. Conclusions

Numerical simulations for manufacturing a honeycomb layer using drape and vacuum thermoformings are presented. The dimensional variation in material distribution depends on history of local displacement and selection of manufacturing process. Prediction of large deformation of fluid material model during inflation phase is important in vacuum forming process. Insufficient mesh density produced unrealistic detailing, incomplete forming and poorly replicate the mould surfaces. It was concluded that the material distribution of drape formed part is virtually insensitive to the mould height and perfectly uniform compared to those of vacuum formed part.

Acknowledgements
Our thanks to the UMP and Ministry of Education, Malaysia for providing the facilities and financial support under the Fundamental Research Grant Scheme RDU130147

References

[1] Throne J L 2008 Understanding thermoforming *Hanser Gardner Publications*
[2] Karamanou M, Warby M K and Whiteman J R 2006 Computational modelling of thermoforming processes in the case of finite viscoelastic materials *Comput. Methods Appl. Mech. Engrg.* **195** 5220–38
[3] Kershner M A and Glacomin A J 2007 Thermoforming cones *Zeitschrift Kunststofftechnik/ Journal of Plastics Technology* **3** 1
[4] Dong Y, Lin R J T and Bhattacharyya D 2005 Determination of critical material parameters for numerical simulation of acrylic sheet forming *J. Mater. Sci.* **40** 399–410
[5] Ó Connor C P J, Martin P J, Sweeney J, Menary G, Caton-Rose P and Spencer P E 2013 Simulation of the plug-assisted thermoforming of polypropylene using a large strain thermally coupled constitutive model *J. Mater. Process. Technol.* **213** 1588–1600.
[6] Lupea I and Cormier J 2007 Size and shape optimization of a polymeric impact energy absorber by simulation *Materiale Plastice* **44** (4) 339–44
[7] Kittikanjanaruk T and Patcharaphun S 2013 Computer Simulation and Experimental Investigations of Wall-Thickness Distribution in High Impact Polystyrene and Amorphous Polyethylene Terephthalate Thermoformed Parts *Kasetsart J. (Nat. Sci.)* **47** 302–9
[8] N. Chevaugeon N, Verron E and Peseux B 2000 Finite element analysis of nonlinear transversely isotropic hyperelastic membranes for thermoforming applications *European Congress on Computational Methods in Applied Sciences and Engineering, Barcelona , ECCOMAS , September 11–14*
[9] Erchiqui F, Gakwaya A and Rachik M 2005 Dynamic finite element analysis of nonlinear isotropic hyperelastic and viscoelastic materials for thermoforming applications *Polymer Engineering and Science* **45** (1) 125–34
[10] Peng X, Yin H, Chen J and and Liu X 2012 A Phenomenological Thermal-Mechanical Viscoelastic Constitutive Modeling for Polypropylene Wood Composites *Advances in Materials Science and Engineering*
[11] Thongwichean T, Phalakornkule C and Chaikittiratana A 2013 Finite Element Analysis for Thermoforming Process of Starch/Biodegradable Polyester Blend *KMUTNB: International Journal of Applied Science and Technology* **5** (2) 33–7
[12] SAS IP. Inc 2011 ANSYS® Polyflow documentation *Release 14.0*